Available online at www.sciencedirect.com
ScienceDirect
Journal of Solid State Chemistry 180 (2007) 1446–1455
JOURNAL OF SOLID STATE CHEMISTRY
www.elsevier.com/locate/jssc

Structural investigation of oxygen non-stoichiometry and cation doping in misfit-layered thermoelectric $(Ca_2CoO_{3-x})(CoO_2)_\delta$, $\delta \approx 1.61$

Chris D. Ling[a,b,*], Karina Aivazian[a], Siegbert Schmid[a], Paul Jensen[a]

[a]*School of Chemistry, The University of Sydney, Sydney, NSW 2006, Australia*
[b]*Bragg Institute, ANSTO, PMB 1, Menai, NSW 2234, Australia*

Received 12 December 2006; received in revised form 12 February 2007; accepted 19 February 2007
Available online 1 March 2007

Astract

The chemical and crystallographic natures of oxygen non-stoichiometry and cation doping in the 'misfit-layered' cobaltate $[Ca_2CoO_{3-x}][CoO_2]_\delta$, $\delta \approx 1.61$, were investigated. Single-phase polycrystalline samples were prepared with the help of a high-energy planetary ball mill, and single crystals grown from a K_2CO_3/KCl flux. Polycrystalline undoped, Ti^{4+}-doped, and Nd^{3+}-doped samples were annealed under both air and under argon in order to modify the oxygen non-stoichiometry. The incommensurately modulated composite crystal structures of undoped and Ti^{4+}-doped single crystals were refined against X-ray diffraction data using the superspace group $X2/m(0,\delta,0)s0$. For the as-made (air-annealed) undoped crystal, 14(2)% oxygen vacancies were found on the disordered O2 site in the central layer of the rock-salt-type subsystem, giving an overall stoichiometry $[Ca_2CoO_{2.86}][CoO_2]_{1.61}$. For the Ti^{4+}-doped crystal this site was found to be almost fully occupied, while Ti^{4+}-dopant cations were located on the disordered Co1 site in the central layer of the rock-salt-type subsystem, giving an overall formula $[Ca_2Co_{0.74}Ti_{0.26}O_{2.98}][CoO_2]_{1.61}$. In both cases, the average cobalt oxidation state is 3.13+. The single-crystal refinements, thermogravimetric analyses and variations in the lattice parameters of polycrystalline samples refined against synchrotron X-ray diffraction (XRD) data indicate that for both undoped and Ti^{4+}-doped samples, substantial numbers of additional oxygen vacancies (15–20%) can be introduced on this site by annealing under an inert atmosphere. Nd^{3+}-doped samples have a much lower tolerance (<5%) for oxygen vacancies.

Keywords: Misfit-layer; Modulated structure; Thermoelectric; Cobaltate; Oxygen non-stoichiometry; Single crystal

1. Introduction

Misfit-layered cobaltates are a family of layered ceramic oxides attracting considerable attention due to their promising thermoelectric properties [1]. Their defining structural feature is the stacking of alternating layer types along the *c*-axis: a pseudo-hexagonal CdI_2-type layer of edge-sharing CoO_6 octahedra (*H* subsystem); and 3 or 4 pseudo-tetragonal rock-salt-type metal oxide layers (RS subsystem). A lattice mismatch between these two types of layers along the *b*-axis (and also along the *a*-axis in some compounds) means that these oxides must be described crystallographically as incommensurately modulated composites.

A large number of misfit-layered cobaltates are known, incorporating various solid solutions of metal ions into the cation sites of the RS subsystem. One of the most intensively studied, commonly known by its approximate empirical formula $Ca_3Co_4O_9$, is notable for its unusually high thermopower [1,2], straightforward synthetic procedure and the presence of only two cation species. Adding to the interest in this phase are observations of giant magnetoresistance [3] and three magnetic transitions [4,5].

Several independent groups have studied the crystal structure of "$Ca_3Co_4O_9$" [6–8] and found it to consist of three layers of stoichiometry CaO/CoO/CaO in the RS subsystem between $[CoO_2]$ layers of the *H* subsystem. The two subsystems are incommensurate along the *b*-axis. The

*Corresponding author. Fax: +61 2 9351 3329.
E-mail address: c.ling@chem..usyd.edu.au (C.D. Ling).

0022-4596/$ - see front matter © 2007 Elsevier Inc. All rights reserved.
doi:10.1016/j.jssc.2007.02.016

misfit parameter $\delta \approx 1.61$ has generally been defined as b_{RS}/b_H. The true stoichiometry is therefore $[Ca_2CoO_3][CoO_2]_\delta$. Three structural polymorphs due to the stacking of $[CoO_2]$ layers in different orientations along the c-axis have been grown as single crystals [7], while only the simplest polymorph has been observed in polycrystalline samples [6,8].

An X-ray absorption near-edge spectroscopy (XANES) study has indicated the presence of cobalt in three oxidation states (II, III, IV) [3], explaining the high electrical conductivity of these materials. Most authors agree that the hexagonal subsystem contains Co^{3+} and Co^{4+} ions, based on total average Co valence, X-ray absorption features and bond length considerations. However, there is some disagreement regarding the formal Co valence in the RS layer $V(Co)_{RS}$. Structural studies considering bond valence sums (BVS) [9] have found $V(Co)_H = 3.5+$, $V(Co)_{RS} = 2.8+$ [7], and $V(Co)_H = 3.39+$, $V(Co)_{RS} = 3.14+$ [8], while X-ray absorption spectroscopy studies have found $V(Co)_{RS}$ much closer to $2+$ [3,10].

Previous considerations of Co valence state based on BVS [7,8] assumed complete occupancy of all oxygen atom sites in the structure. Recently, however, the overall oxygen content of as-made (air-annealed) samples has been determined by cerimetric and iodometric titration [11–13], finding an average Co valence of $\sim 3.16+$. This value is lower than expected ($3.23+$) if complete oxygen stoichiometry is assumed in both layers, i.e., there are a significant number of oxygen vacancies in these samples. Furthermore, the oxygen content was found to vary according to synthetic procedure, suggesting a possible means of controlling the physical properties—the thermoelectric power was found to increase with the number of oxygen vacancies. Annealed under a mildly reducing atmosphere (N_2 or Ar), the oxygen content decreases by $\sim 2.6\%$ [11,12]. The location of the oxygen vacancies within the structure has not been investigated, but they have generally been assumed to reside in the RS subsystem. In this report, the phase will from now on be referred to as $[Ca_2CoO_{3-x}][CoO_2]_\delta$, $\delta \approx 1.61$.

The goal of this investigation was to identify and quantify the site(s) of oxygen non-stoichiometry in $[Ca_2CoO_{3-x}][CoO_2]_\delta$. In addition, several types of cation doping were investigated for their effects on the structure and on oxygen non-stoichiometry (and hence, on cobalt valence state). There are many reports in the literature of cation doping in $[Ca_2CoO_{3-x}][CoO_2]_\delta$, both for $Co^{2+/3+/4+}$ (e.g., Ti^{4+} [14,15], $Mn^{2+/3+/4+}$ [16]) and for Ca^{2+} (e.g., Sr^{2+} [17,18], Ba^{2+} [19], La^{3+} [20], Y^{3+} [21], Bi^{3+} [2]). Here, we have focused on charge effects in the RS subsystem, by doping Nd^{3+} for Ca^{2+} (Nd-doping has not been previously reported, but was deliberately chosen here because its ionic radius (0.983 Å) is close to that of Ca^{2+} (1.00 Å) [22]); and Co valence effects by doping Ti^{4+} for $Co^{2+/3+/4+}$. Note that the site of Ti-doping for Co has not itself been resolved, having been proposed to occur in the H subsystem based on consideration of ionic radii [15] and in the RS subsystem based on changes in magnetic and transport properties [14].

2. Experimental

All samples were prepared using commercially supplied reagents. TiO_2 (Sigma-Aldrich, 4N5) was used as purchased. Nd_2O_3 (Sigma-Aldrich 3N) was dehydrated overnight at 1000 °C. $CaCO_3$ (Aithaca 5N) was dehydrated overnight at 600 °C. Co_3O_4 (Aithaca 5N) was annealed in air at 600 °C in order to remove any CoO impurity.

Synchrotron powder X-ray diffraction (XRD) data ($\lambda = 0.80088$ Å) were collected at the Australian National Beamline Facility, Photon Factory, Japan. Samples were placed in rotating 0.3 mm glass capillaries and data collected on image plates spanning 5–50° 2θ in Debye–Scherrer geometry.

Energy-dispersive X-ray analyses (EDXA) were performed in conjunction with imaging using a Phillips XL-30 scanning electron microscope (SEM) with a tungsten filament operating at 20 keV, a spot size setting of 5 and a working distance of 11 mm.

2.1. Polycrystalline samples

Polycrystalline $[Ca_2CoO_{3-x}][CoO_2]_\delta$, $\delta \approx 1.61$, was prepared by conventional solid-state reaction from stoichiometric quantities of $CaCO_3$ and Co_3O_4. Samples were ground using an agate mortar and pestle, fired at 900 °C for 24 h, then reground and pressed into pellets prior to a second firing at 900 °C for 24 h. Purity was confirmed by XRD and EDXA (Table 1).

Polycrystalline samples of $[Ca_{1.7}Nd_{0.3}CoO_{3-x}][CoO_2]_{1.62}$ and $[Ca_2Co_{0.55}Ti_{0.45}O_{3-x}][CoO_2]_{1.61}$ were initially prepared in the same manner as the undoped sample, from stoichiometric quantities of $CaCO_3$, Co_3O_4, Nd_2O_3, and TiO_2. Small impurities were observed by XRD: $NdCoO_3$ and $Ca_3Co_2O_6$ for the Nd-doped sample; and $CaCO_3$, Co_3O_4, and TiO_2 for the Ti-doped sample. These impurities were eliminated by grinding the samples for 12 h in a tungsten-carbide jar at 350 rpm using a high-energy planetary ball-mill (Retsch PM100) before re-firing as pellets at 900 °C for 24 h. Phase purity and composition was confirmed by XRD and EDXA (Table 1).

Following their synthesis and initial characterization, half of each sample was annealed in an oxidizing atmosphere (air) and the other half in a reducing atmosphere

Table 1
Results of EDXA compositional analyses of polycrystalline samples

	Co (%)	Ca (%)	Nd (%)	Ti (%)	Repeats
$[Ca_2CoO_{3-x}][CoO_2]_{1.61}$	56±2	44±2	—	—	11
$[Ca_{1.7}Nd_{0.3}CoO_{3-x}][CoO_2]_{1.62}$	56±1	38±1	6±1	—	10
$[Ca_2Co_{0.55}Ti_{0.45}O_{3-x}][CoO_2]_{1.61}$	49±3	43±2	—	8±2	17

(flowing argon) to vary the oxygen content. In both cases, samples were re-ground, heated to 600 °C for 15 h, and cooled slowly (0.5 °C/min) to room temperature.

TGA experiments were performed on all polycrystalline samples with a TA Instruments Hi-Res TGA 2950 Thermogravimetric Analyzer, using a heating rate of 0.7 °C/min. Industrial-grade oxygen and high-purity nitrogen were used to oxygenate and deoxygenate samples, respectively. TGA curves were collected under nitrogen (for all air-annealed samples) and under oxygen (for argon-annealed samples). Fig. 1 shows the masses gained as argon-annealed samples of undoped, Nd^{3+}-doped and Ti^{4+}-doped samples were heated and cooled under flowing oxygen. The masses gained correspond to a 2.1% increase in oxygen content of the undoped sample, a 0.7% increase in oxygen content of the Nd^{3+}-doped sample, and a 2.5% increase in oxygen content of the Ti^{4+}-doped sample. Note that for the undoped and Ti^{4+}-doped compounds, dips in the TGA curves at high temperature indicate that an oxygen-deficient form is more stable at high temperature; this is in agreement with previous reports.

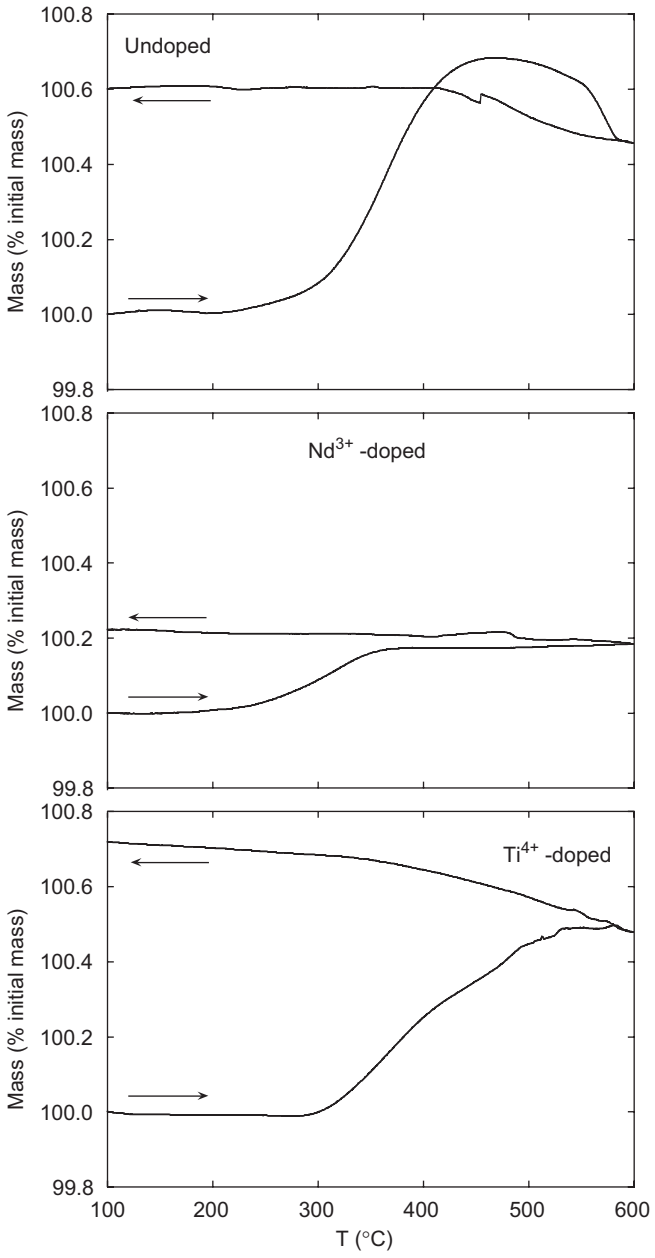

Fig. 1. TGA curves under flowing oxygen for undoped (top), Nd^{3+}-doped (middle), and Ti^{4+}-doped (bottom) argon-annealed polycrystalline samples of $[Ca_2CoO_{3-x}][CoO_2]_{1.61}$.

2.2. Single crystals

Single crystals of $[Ca_2CoO_{3-x}][CoO_2]_{1.61}$ and $[Ca_2Co_{1-y}Ti_yO_{3-x}][CoO_2]_{1.61}$ were grown from stoichiometric mixtures of $CaCO_3$, Co_3O_4, and TiO_2 (assuming the same stoichiometry as the polycrystalline samples, i.e., $y = 0.45$) in a 4:1 K_2CO_3/KCl flux, with a total solute concentration of 1.5 mol%. The homogenized mixture was transferred to a lidded alumina crucible and fired at 950 °C for 20 h, then cooled to 650 °C at a rate of 5 °C/h, and then to room temperature at a rate of 100 °C/h. Grown crystals were collected by dissolving the flux in water. Grown crystals were thin hexagonal plates with dimensions of up to $2 \times 2 \times 0.2\,mm^3$.

After testing a number of crystals of $[Ca_2CoO_{3-x}][CoO_2]_{1.61}$ and $[Ca_2Co_{0.55}Ti_{0.45}O_{3-x}][CoO_2]_{1.61}$, untwined single crystals were identified and diffraction data collected on a Bruker-Nonius FR591 Kappa Apex II diffractometer, using Mo-K_α ($\lambda = 0.71073$ Å) radiation from a rotating anode generator. Data were collected at 150 K, cooled with the Oxford 700+ cryostream, using a 2 kW setting for 11 h ($[Ca_2CoO_{3-x}][CoO_2]_{1.61}$) or 24 h ($[Ca_2Co_{0.55}Ti_{0.45}O_{3-x}][CoO_2]_{1.61}$). Matrix collections were performed to determine unit cells. Both crystals were found to be of the simplest polymorph (Phase 1) described by Lambert et al. [7]. This is the only polymorph observed in diffraction from polycrystalline samples, however, no full refinements using single-crystal diffraction data have been reported. Indexing was carried out using the Bruker–Nonius *Cell Now* program. For each crystal, a full sphere of data was collected for $\sin\theta/\lambda \leqslant 1.2$, yielding >2700 unique observed reflections from the subsystems, i.e., $(h\,k\,l\,0)$ and $(h\,0\,l\,m)$; however, as in the powder XRD data, no satellite reflections were observed of the type $(h\,k\,l\,m)$ where $k \neq 0$ and $m \neq 0$. An absorption correction was performed using the Bruker–Nonius *TwinAbs* program, treating the two subsystems as twin domains in order to ensure correct scaling of the data. Data collection details are presented in Table 2.

3. Structure refinements

All structure refinements (Rietveld and single crystal) were carried out using the *Jana2000* program [23]. Starting structural parameters were taken from Grebille et al. [6]; however, in this study we have used the superspace group

Table 2
Details of single crystal data collection for $[Ca_2CoO_{3-x}][CoO_2]_\delta$ and $[Ca_2Co_{1-y}Ti_yO_{3-x}][CoO_2]_\delta$

Formula	$[Ca_2CoO_{3-x}][CoO_2]_\delta$	$[Ca_2Co_{1-y}Ti_yO_{3-x}][CoO_2]_\delta$
Crystal shape and size (mm)	Plate $0.23 \times 0.13 \times 0.05$	Plate $0.23 \times 0.16 \times 0.03$
Superspace group	$X2/m(0,\delta,0)s0$	$X2/m(0,\delta,0)s0$
a (Å)	4.8381(2)	4.8414(3)
b_{RS} (Å)	4.5347(2)	4.5317(3)
c (Å)	10.8558(3)	10.8766(6)
$>$ (o)	98.1136(15)	98.127(3)
$\delta = b_{RS}/b_H$	1.6053(3)	1.6032(4)
Z	2	2
λ (g cm^{-3}), μ (cm^{-1})	4.656, 11.13	4.640, 10.73
λ (Å)	0.71073	0.71073
$(\sin\theta/\lambda)_{max}$	1.2	1.2
Data collection temperature (K)	150	150
Refined parameters	61	62
Total reflections (all, $I \geqslant 3\sigma I$)	13 165, 11 740	15 973, 14 933
Unique reflections (all, $I \geqslant 3\sigma I$)	3076, 2804	2739, 2604
R_{int} (after absorption correction)	0.0278	0.0385
R, wR	0.0241, 0.0256	0.0299, 0.0282
Goodness of fit	3.42	7.04

The relationship between the two subsystems was defined in the refinement program *Jana2000* [23] by the second composite matrix 1000/0001/0010/0100.

$X2/m(0,\delta,0)s0$, which is the standard setting of the superspace group $C2/m(1,\delta,0)s0$ used by Grebille et al.[1]

3.1. Lattice parameters from XRD

A Rietveld-refinement was carried out against synchrotron powder XRD data collected from the air-annealed polycrystalline sample of $[Ca_2CoO_{3-x}][CoO_2]_{1.61}$, using the structural parameters from Grebille et al. [6]. In the first instance, the only parameters refined were the unit cell, global isotropic atomic displacement parameters (ADPs) for each atom type, peak shape, background, and an instrumental zero-offset. Fig. 2 shows the final observed, calculated and difference profiles ($R_p = 0.0415$, w$R_p = 0.0606$). Note that no significant intensity is observed for any satellite peak of the type ($h\,k\,l\,m$), $k \neq 0$ and $m \neq 0$. Green reflection markers (the lower row) indicate the positions of the first-order satellites for which $k \neq 0$ and $m = 1$, or $k = 1$ and $m \neq 0$. The extremely weak nature of these satellites is in agreement with all previous structural studies, none of which observed them in powder diffraction data (including neutron powder diffraction data) [6–8]. Rietveld-refinement of atomic positional and modulation parameters was stable, however, large standard deviations on these final refined parameters indicated that the results were unreliable.

Several unindexed reflections remained after Rietveld-refinement, labeled (● and *) in Fig. 2. These were also noted by Grebille et al., who suggested that they might be due to an additional modulation along the (0.3, 1, 0) direction of the RS subsystem. We do not observe enough reflections in the powder XRD data to adequately test this possibility, and no statistically significant intensity was observed at the corresponding positions in single-crystal X-ray diffraction data (see Section 3.2 below). Furthermore, we note in Fig. 2 that the two reflections labeled "●" have quite different shapes and intensities, whereas in Fig. 3 of Grebille et al. they have quite similar shapes and intensities. This suggests that they should not be treated as arising due to the same modulation, and may instead be due to small (unidentified) impurities. [Note that although the reflection labeled "*" falls close to a satellite reflection marker, this appears to be a coincidence.]

Finally, reference should be made to the triclinic symmetry-lowering observed by Grebille et al., characterized by a splitting of the (1 1 2 0) reflection. As can be seen in the inset to Fig. 2, we do not observe this splitting (cf. inset to Fig. 3 of Grebille et al., noting that the two data sets were collected at different synchrotron X-ray wavelengths). The difference between the symmetries of the two samples is unclear, but presumably related to the use of slightly different synthetic conditions.

Synchrotron powder XRD data were used to refine unit cell parameters for all the polycrystalline samples prepared in this study, in the same manner as described above for the undoped sample. Table 3 compares unit cell parameters of air-annealed and argon-annealed samples of the same composition, and Table 4 compares unit cell parameters of the air-annealed undoped sample to those of the air-annealed Nd- and Ti-doped samples.

3.2. Single-crystal refinement of $[Ca_2CoO_{3-x}][CoO_2]_{1.61}$

Structure refinement of $[Ca_2CoO_{3-x}][CoO_2]_{1.61}$ started from the model of Grebille et al. [6]. This model includes positional modulation waves for all atoms except the Co and O atoms in the central layer of the RS subsystem (Co1 and O2), for which split site disorder models were used. All parameters in this model could be refined, as well as the z-coordinates of Co1a and O2b, which were previously fixed. The final refined structure was essentially identical to that reported by Grebille et al. using neutron and X-ray powder diffraction data, but with significantly higher accuracy.

Attempts to replace the split-site disorder model of the central layer of the RS subsystem (Co1 and O2) with positional modulation waves, including so-called sawtooth functions, were unsuccessful. The disorder model yielded $R_{obs} = 2.41$, while removing the disorder yielded $R_{obs} = 10.07$. Positional modulation waves on both the

[1]Note that the structural parameters in Table 2 of Grebille et al. correspond to the $X2/m(0,\delta,0)s0$ rather than the $C2/m(1,\delta,0)s0$ setting; hence, no transformation of those co-ordinates was applied.

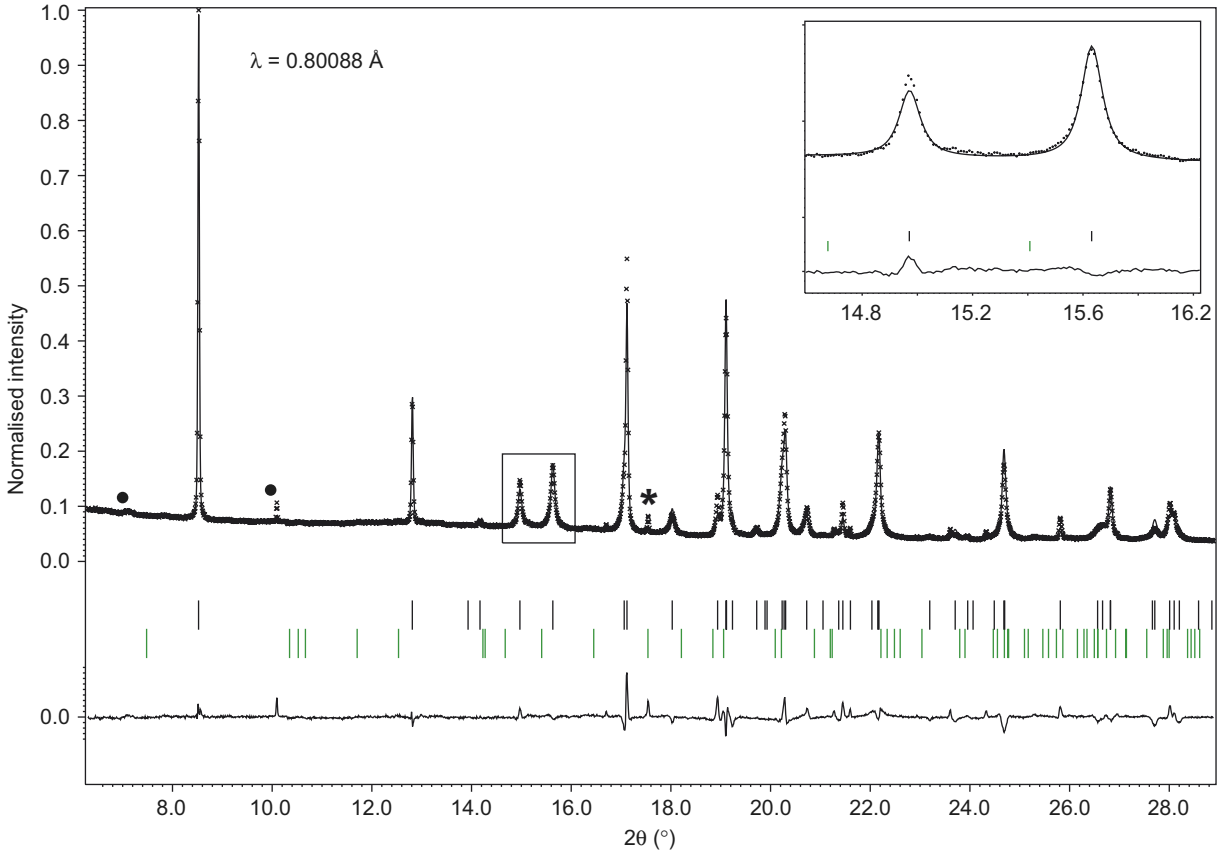

Fig. 2. Observed (dotted line), calculated (solid line) and difference synchrotron XRD profiles ($\lambda = 0.80088$ Å) for the final Rietveld-refinement of air-annealed polycrystalline $[Ca_2CoO_{3-x}][CoO_2]_{1.61}$. Bragg reflections are indicated by an upper row of black tick marks (main reflections) and a lower row of green tick marks (first-order satellites). The unindexed marked peaks (● and *) are discussed in the text. The enlarged portion of the pattern (inset) shows no sign of a previously reported symmetry-lowering. Overall powder R-factors: $R_p = 0.0415$ w$R_p = 0.0606$.

Table 3
Refined lattice parameters for all air- and argon-annealed samples, highlighting the percentage unit cell changes after argon-annealing

	a (Å)	b (Å)	c (Å)	β (°)	$\delta = b_{RS}/b_H$
Air-$[Ca_2CoO_{3-x}][CoO_2]_\delta$	4.8373(4)	4.5465(5)	10.8595(9)	98.117(2)	1.6110(1)
Argon-$[Ca_2CoO_{3-x}][CoO_2]_\delta$	4.8381(4)	4.5268(6)	10.8646(8)	98.113(3)	1.6025(2)
% change	0.02	−0.44	0.05	0.00	−0.53
Air-$[Ca_{1.7}Nd_{0.3}CoO_{3-x}][CoO_2]_\delta$	4.8481(4)	4.5745(6)	10.8496(9)	98.181(2)	1.6201(2)
Argon-$[Ca_{1.7}Nd_{0.3}CoO_{3-x}][CoO_2]_\delta$	4.8518(4)	4.5738(6)	10.8519(8)	98.183(2)	1.6197(2)
% change	0.08	−0.02	0.02	0.00	−0.02
Air-$[Ca_2Co_{0.55}Ti_{0.45}O_{3-x}][CoO_2]_\delta$	4.8330(2)	4.5446(5)	10.8814(6)	98.100(3)	1.6114(3)
Argon-$[Ca_2Co_{0.55}Ti_{0.45}O_{3-x}][CoO_2]_\delta$	4.8383(4)	4.5385(7)	10.8863(9)	98.130(4)	1.6073(3)
% change	0.11	−0.13	0.05	0.03	−0.26

Table 4
Refined lattice parameters for undoped and doped samples, highlighting the percentage unit cell changes after cation doping

	a (Å)	b (Å)	c (Å)	β (°)	$\delta = b_{RS}/b_H$
Air-$[Ca_2CoO_{3-x}][CoO_2]_\delta$	4.8373(4)	4.5465(5)	10.8595(9)	98.117(2)	1.6110(1)
Air-$[Ca_{1.7}Nd_{0.3}CoO_{3-x}][CoO_2]_\delta$	4.8481(4)	4.5745(6)	10.8496(9)	98.181(2)	1.6201(2)
% change	0.22	0.61	−0.05	0.09	0.56
Air-$[Ca_2CoO_{3-x}][CoO_2]_\delta$	4.8373(4)	4.5465(5)	10.8595(9)	98.117(2)	1.6110(1)
Air-$[Ca_2Co_{0.55}Ti_{0.45}O_{3-x}][CoO_2]_\delta$	4.8330(2)	4.5446(5)	10.8814(6)	98.100(3)	1.6114(3)
% change	−0.09	−0.04	0.20	−0.02	0.02

Table 5
Atomic positions, occupancies, ADP's, the first and second harmonics of the sin (s) and cos (c) terms of the modulation waves for $[Ca_2CoO_{3-x}][CoO_2]_\delta$ obtained by refinement of single crystal X-ray diffraction data

Atom	Modulation	x (a)	y (b)	z (c)	Occupancy	U_{11}	U_{22}	U_{33}	U_{13}
RS subsystem									
Co1a		0	0	0.5	0.2568(12)	0.00553(14)	0.0133(2)	0.00254(10)	0.00024(13)
Co1b		0.08480(12)	0.06321(13)	0.4999(5)	0.7432(12)	0.00553(14)	0.0133(2)	0.00254(10)	0.00024(13)
Ca		0.42939(5)	0	0.27054(2)	1	0.00512(8)	0.00682(6)	0.00537(6)	0.00060(6)
	s,1	−0.01788(14)	0	0.00052(7)					
	c,1	0	−0.0017(3)	0					
	s,2	0	0.0009(2)	0					
	c,2	0.0009(2)	0	0.00223(10)					
O1		0.05233(19)	0	0.66214(9)	1	0.0079(3)	0.0084(3)	0.0102(3)	0.0013(2)
	s,1	−0.0028(7)	0	−0.0007(3)					
	c,1	0	0.0003(10)	0					
	s,2	0	−0.0022(9)	0					
	c,2	0.0008(10)	0	−0.0000(5)					
O2a		0.0988(8)	0.5	0.4999(3)	0.467(7)	0.0123(11)	0.0046(6)	0.0046(6)	0.0004(7)
O2b		0	0.5696(10)	0.5	0.389(6)	0.0123(11)	0.0046(6)	0.0046(6)	0.0004(7)
H subsystem									
O3		0.38612(11)	0.75	−0.09370(5)	1	0.00286(14)	0.00427(16)	0.00384(16)	0.00040(12)
	s,1	0	0.0008(12)	0					
	c,1	0.0062(4)	0	0.00342(16)					
	s,2	0	0.0073(9)	0					
	c,2	0.0015(4)	0	0.00217(18)					
Co2		0.75	0.75	0	1	0.00170(3)	0.00292(4)	0.00245(4)	0.00037(3)
	s,1	0	0	0					
	c,1	0.00501(9)	0	0.00416(4)					
	s,2	0	−0.0013(2)	0					
	c,2	0	0	0					

The total occupancy of the Co1a and Co1b sites was constrained to 100%, and the ADP's of the split Co1a/Co1b and O2a/O2b sites were constrained to be equal. Note that $U_{12} = U_{23} = 0$ for all sites.

Co1 and O2 sites only reduced the R_{obs} value to 9.98, and the introduction of sawtooth functions yielded no further improvement. Attempts were also made to refine the structure reported by Miyazaki et al. [8], which included pronounced positional modulations waves on all atomic sites, but meaningful results could not be obtained due to the absence of observed satellite reflections.

Refinement of fractional occupancies of each of the oxygen atom sites indicated full occupancy of O1 (in the H subsystem) and O3 (on the outer CaO layers of the RS subsystem), which were subsequently fixed at 100%. However, significantly reduced occupancy was found for the split O2 site (in the central CoO layer of the RS subsystem), the total O2 occupancy refining to 86(2)%, i.e., $x = 0.14(2)$ in $[Ca_2CoO_{3-x}][CoO_2]_{1.61}$. Final refinement statistics are presented in Table 2, refined parameters in Table 5, and the structure is shown in Fig. 3.

As a final check on the validity of the refined structure model, it was used to calculate the intensities of satellite reflections of the type ($hklm$), $k \neq 0$ and $m \neq 0$, none of which were observed ($>3\sigma$) in the single-crystal X-ray data. The strongest such satellite reflections, $\langle 1\,2\,0\,\bar{1}\rangle$ and $\langle \bar{1}\,2\,2\,\bar{1}\rangle$, had calculated intensities $<0.1\%$ that of the strongest parent reflections. Moreover, these (relatively) strong satellite reflections occur at low diffraction angles where background noise on the detector is highest. The failure to observe statistically significant intensity in these reflections is therefore entirely consistent with the refined structure model.

3.3. Single-crystal refinement of $[Ca_2Co_{1-y}Ti_yO_{3-x}][CoO_2]_{1.61}$

The changes in unit cell parameters of the Ti-doped single crystal compared to the undoped single crystal (Table 2) are in good agreement with the changes observed for Ti-doping in polycrystalline samples by powder XRD (Table 4) (the layer-stacking c-axis being most strongly affected). This strongly supports the presence of Ti in the flux-grown single crystal.

In order to identify the site(s) and extent of Ti-doping, refinement of the structure of $[Ca_2Co_{1-y}Ti_yO_{3-x}][CoO_2]_{1.61}$ was carried out in the same manner as for $[Ca_2CoO_{3-x}][CoO_2]_{1.61}$, mixed Ti/Co occupancy was refined for each of the Co sites. The Co2 site in the H subsystem refined to less than 0.3% Ti (subsequently fixed to 100% Co), while the refinement indicated the presence of a significant amount of Ti on the Co1 site in the RS subsystem. Unfortunately, the split-site model for Co1 means that Co:Ti ratios in the Co1a and Co1b sites cannot be meaningfully refined at the same time as the Co1a:Co1b ratio. In this investigation, the compromise method used to refine the Co:Ti ratio was to

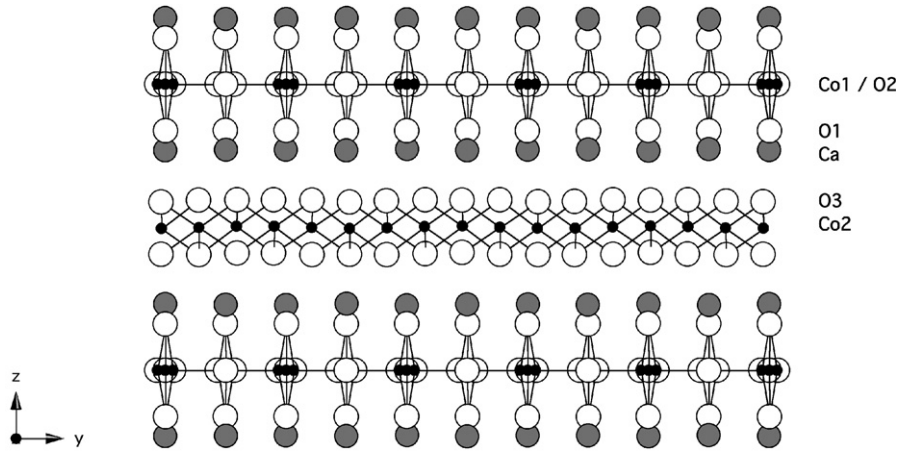

Fig. 3. The final refined structure of $[Ca_2CoO_{2.86}][CoO_2]_{1.61}$, viewed along x. Co atoms are black, Ca atoms are gray, and O atoms are white. Note the split-site disorder models for the Co1 and O2 sites in the middle layer of the RS subsystem.

first refine the Co1a:Co1b ratio without the restriction that both site occupancies add up to 100%. The total Co1 occupancy then converged to 94.8(8)%. Assuming that there are no cation vacancies in the structure, the difference in X-ray scattering factors of Co and Ti could then be used to calculate the total titanium occupancy on the Co1 split site as 25.9(8)%, i.e., $y = 0.259(8)$ in $[Ca_2Co_{1-y}Ti_yO_{3-x}][CoO_2]_{1.61}$. This is somewhat lower than the nominal value ($y = 0.45$) expected from the stoichiometry of the reactants placed in the flux. This level of doping is equivalent to 9.9% total Ti-doping for Co in the structure. It was necessary to assume that the Co:Ti ratio was identical on the Co1a and Co1b site.

Final refinement statistics are presented in Table 2, and refined parameters in Table 6. Note that in contrast to the refinements results for the undoped crystal, the total O2 occupancy refined to 98(2)%, i.e., $x = 0.02(2)$ in $[Ca_2Co_{0.74}Ti_{0.26}O_{3-x}][CoO_2]_{1.61}$.

4. Discussion

The TGA results for the undoped sample (Fig. 1) are in agreement with those recently reported [11,12]. The results for the Nd^{3+}-doped (for Ca^{2+}) sample indicate a reduced tolerance for oxygen vacancies, as expected, due to the higher total cation charge relative to the number of oxygen anion sites. The results for the Ti^{4+}-doped (for $Co^{2+/3+/4+}$) sample, on the other hand, indicate a higher tolerance for oxygen vacancies despite the higher total cation charge. This can be understood in light of the single-crystal refinement results, which show that the air-annealed Ti^{4+}-doped compound has a higher oxygen content (total O2 occupancy refining to 98(2)%) compared to the air-annealed undoped compound (total O2 occupancy refining to 86(2)%). The TGA data showed a 2.1% change in oxygen content of the undoped sample, a 0.7% change in oxygen content of the Nd^{3+}-doped sample, and a 2.5% change in oxygen content of the Ti^{4+}-doped sample. Since the changes in lattice parameters after argon-annealing (Table 3) indicate that these additional vacancies are in all cases located on the O2 site, the argon-annealed Ti^{4+}-doped compound actually contains approximately the same number of oxygen vacancies on that site (total O2 occupancy ~86%) as the air-annealed undoped compound; while argon-annealing of the undoped compound roughly doubles the vacancy concentration on that site (total O2 occupancy ~73%). Argon-annealing of the Nd^{3+}-doped sample leads to a reduced number of vacancies (total O2 occupancy ~96%).

Comparing lattice parameters of air-annealed and argon-annealed samples in Table 3, we find that for the undoped and Ti^{4+}-doped compounds, b increases by ~0.5% while δ increases in proportion (i.e., b_{RS} increases while b_H stays constant). This strongly indicates that oxygen vacancies are located in the RS subsystem, supporting the single-crystal refinement results in which 14(2)% oxygen vacancies were located on the O2 split site in the central layer of the RS subsystem. For the Nd^{3+}-doped compound, very little change in the unit cell is observed, in accordance with the TGA evidence that this compound has a greatly reduced tolerance for oxygen vacancies.

Comparing lattice parameters of doped and undoped samples, we find that after Nd^{3+}-doping, b_{RS} and δ increase by similar amounts, implying that b_H stays approximately constant. This indicates that the RS subsystem is more affected than the H subsystem by Nd^{3+}-doping—i.e., by increased oxygen content—providing further evidence that oxygen vacancies are located in the RS subsystem. (Note that this is not a cation size effect—Nd^{3+} and Ca^{2+} have very similar ionic radii of 0.983 and 1.00 Å, respectively [22].) After Ti^{4+}-doping, however, we find that c expands while b_{RS} and δ are relatively unaffected (as reported [14]). This effect is more difficult to interpret, because c is the stacking axis, and is therefore affected by both the RS and H subsystems. In order to clarify this effect, we must examine the bond lengths within each subsystem as obtained from

Table 6
Atomic positions, occupancies, ADP's, the first and second harmonics of the sin (s) and cos (c) terms of the modulation waves for $[Ca_2Co_{1-y}Ti_yO_{3-x}][CoO_2]_\delta$ obtained by refinement of single crystal X-ray diffraction data

Atom	Modulation	x (a)	y (b)	z (c)	Occupancy	U_{11}	U_{22}	U_{33}	U_{13}
RS subsystem									
Co/Ti1a		0	0	0.5	0.237(2)	0.0079(3)	0.0135(4)	0.00089(12)	0.0001(2)
Co/Ti1b		0.07600(18)	0.05724(18)	0.49997(6)	0.763(3)	0.0079(3)	0.0135(4)	0.00089(12)	0.0001(2)
Ca		0.42943(6)	0	0.27164(2)	1	0.00421(10)	0.00496(8)	0.00461(7)	0.00054(6)
	s,1	−0.01708(18)	0	0.00038(8)					
	c,1	0	−0.0015(4)	0					
	s,2	0	0.0008(2)	0					
	c,2	0.0006(2)	0	0.00206(10)					
O1		0.0529(2)	0	0.66405(9)	1	0.0074(3)	0.0063(3)	0.0086(3)	0.0011(3)
	s,1	−0.0015(8)	0	−0.0007(3)					
	c,1	0	−0.0025(13)	0					
	s,2	0	−0.0014(9)	0					
	c,2	−0.0000(11)	0	−0.0001(5)					
O2a		0.0886(11)	0.5	0.5000(4)	0.532(12)	0.0105(16)	0.021(2)	0.0045(7)	0.0015(13)
O2b		0	0.5630(15)	0.5	0.448(12)	0.532(12)	0.0105(16)	0.021(2)	0.0045(7)
H subsystem									
O3		0.38618(14)	0.75	−0.09335(6)	1	0.00236(19)	0.0027(2)	0.0034(18)	0.00043(15)
	s,1	0	0.0035(17)	0					
	c,1	0.0067(4)	0	0.00307(17)					
	s,2	0	0.0063(10)	0					
	c,2	0.0010(5)	0	0.00218(19)					
Co2		0.75	0.75	0	1	0.00095(5)	0.00166(5)	0.00171(5)	0.000314(4)
	s,1	0	0	0					
	c,1	0.00554(10)	0	0.00422(4)					
	s,2	0	−0.0016(3)	0					
	c,2	0	0	0					

The total occupancy of the Co1a and Co1b sites was constrained to 100%, and the ADP's of the split Co1a/Co1b and O2a/O2b sites were constrained to be equal. The Ti:Co ratio on the Co/Ti1a and Co/Ti1b sites was refined in an independent step, described in the Section 3.3, as 25.9(8) % Ti. Note that $U_{12} = U_{23} = 0$ for all sites.

single-crystal refinement. In fact, there is a 1.7% increase in the Co1⋯O1 bond length (RS) after Ti^{4+}-doping (from 1.736(9) to 1.766(4) Å), while the corresponding change in the Co2⋯O3 bond (H) is only 0.3% (from 1.9049(9) to 1.9111(4) Å). Thus, the RS subsystem is more strongly affected by Ti^{4+} substitution than the H subsystem, suggesting that Ti^{4+} is preferentially doped into the RS subsystem. This supports the result obtained by refining occupancies. Note that although the crystal (grown from a flux) refines to $y = 0.259$ compared to the nominal $y = 0.450$ for the powder sample, the fact that the change in unit cell compared to the undoped samples is almost exactly the same (~0.2% increase in c) for the crystals as for the powder suggests that the powder sample may have contained some undetected impurities.

BVS[2] [9] provide further support for the presence of Ti^{4+} in the RS subsystem. Fig. 4 shows that the undoped compound has average valences of $Co2^{3.3+}$ and a $Co1^{2.4+}$. This is consistent with previous studies, most of which agree that Co^{3+} and Co^{4+} are found in the hexagonal subsystem, while Co^{2+} is in the RS subsystem [3,7]. Fig. 4 also shows that O2 in the RS subsystem (the site of oxygen vacancies) is the most underbonded oxygen site, while O3 in the H subsystem is slightly overbonded. In the Ti^{4+}-doped compound, modeling Ti^{4+} in the H subsystem results in greater overbonding of both O3 and of Ti^{4+} (BVS = ~4.6, not shown in Fig. 4). No expansion of the H subsystem, which would relieve this overbonding, is observed. Modeling Ti^{4+} in the RS subsystem, however, leaves it slightly underbonded, a situation that could be relieved by local distortions (which would not be seen in the diffraction data).

Finally, it is interesting to note that the refined stoichiometries of the undoped and Ti^{4+}-doped single crystals, $[Ca_2CoO_{2.86}][CoO_2]_{1.61}$ and $[Ca_2Co_{0.74}Ti_{0.26}O_{2.98}][CoO_2]_{1.61}$, both imply an average cobalt oxidation state of 3.13+. Since these crystals were grown out of a flux, and the composition of the Ti^{4+}-doped crystal was in fact slightly different to the nominal ratio of cation species placed in the flux, this suggests that an average cobalt oxidation state of 3.13+ is particularly stable. The thermopower of these compounds has been reported to improve with both oxygen annealing [11] and Ti-doping [14], however, these results show that Ti^{4+}-doping does not change the average oxidation state of cobalt in the way that oxygen-annealing does. The oxygen content itself, which is

[2]Note that split sites (O2a/O2b, Co1a/Co1b, Ti1a/Ti1b) have been used to model disorder in the central layer of the RS subsystem; therefore, the BVS curves for the a/b components represent continuous ranges of values.

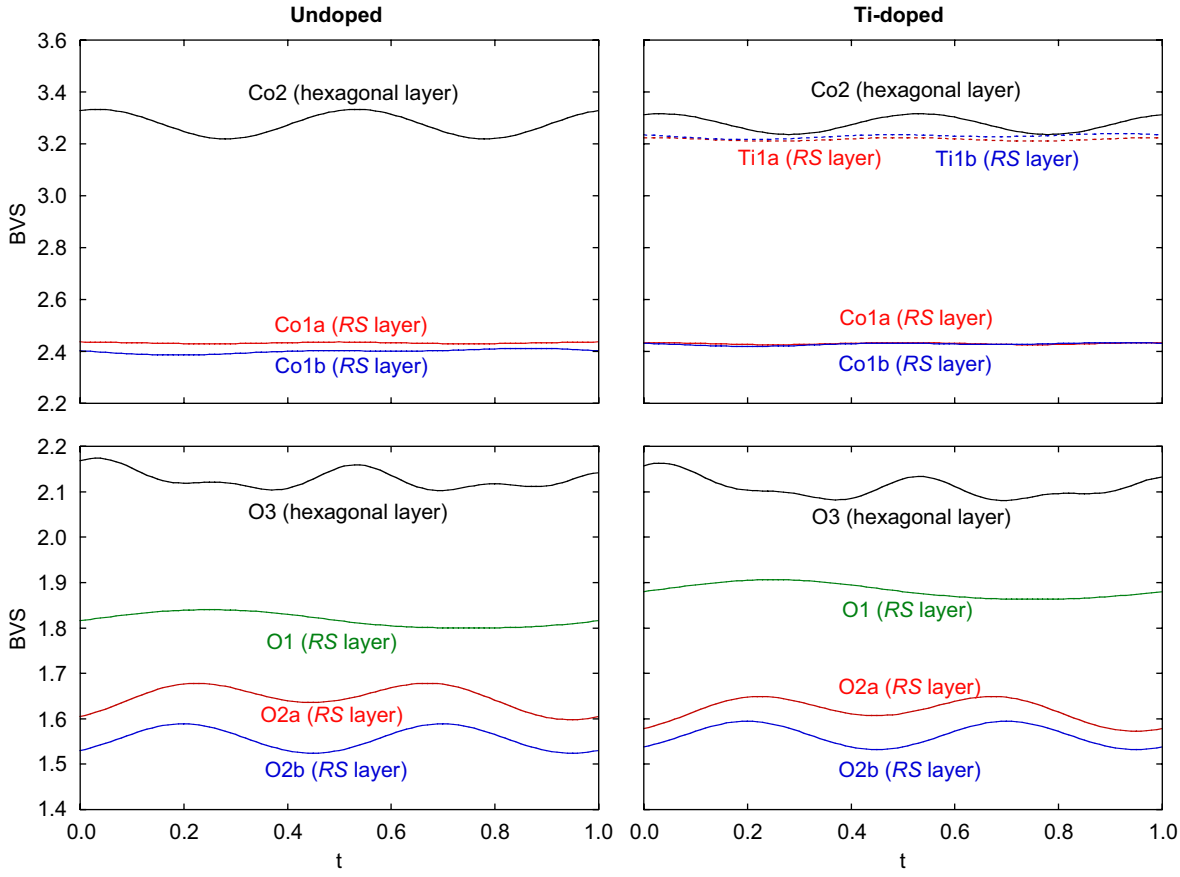

Fig. 4. Bond valence sums (BVS) for the final refined structures of $[Ca_2CoO_{2.86}][CoO_2]_{1.61}$ and $[Ca_2Co_{0.74}Ti_{0.26}O_{2.98}][CoO_2]_{1.61}$, as functions of the internal coordinate t along the modulation direction b in real space. Note that split sites (O2a/O2b, Co1a/Co1b, Ti1a/Ti1b) have been used to model disorder in the central layer of the RS subsystem; therefore, the BVS curves for the a/b components represent continuous ranges of values.

increased in both cases, may therefore be a critical factor in determining thermopower.

5. Conclusions

The structural model of $[Ca_2CoO_{3-x}][CoO_2]_{1.61}$ ("$Ca_3Co_4O_9$") proposed and refined against powder X-ray and neutron diffraction data by Grebille et al. [6] has been confirmed and further developed by single-crystal X-ray diffraction. In particular, the oxygen vacancies responsible for the observed non-stoichiometry x have now been located on the disordered O2 site in the central layer of the RS subsystem. As-made samples contain 14(2)% oxygen vacancies on this site, with TGA results indicating that a further ~13% vacancies (assuming that they occur on the same site) can be introduced by high-temperature annealing under argon or nitrogen atmospheres. Doping Nd^{3+} for Ca^{2+} substantially reduces the tolerance of the structure for oxygen vacancies to ~4% on the O2 site, as expected due to the increased total cation charge.

Doping Ti^{4+} for $Co^{2+/3+/4+}$ decreases the number of oxygen vacancies while maintaining the same average cobalt oxidation state—the refined stoichiometries of the undoped and Ti^{4+}-doped single crystals, $[Ca_2CoO_{2.86}][CoO_2]_{1.61}$ and $[Ca_2Co_{0.74}Ti_{0.26}O_{2.98}][CoO_2]_{1.61}$, both imply an average cobalt oxidation state of 3.13+. Ti^{4+} is located on the disordered Co1 site in the central layer of the RS subsystem. As-made (air-annealed) Ti^{4+}-doped samples contain essentially no oxygen vacancies, however, TGA results indicate that the argon-annealed Ti^{4+}-doped samples contains approximately the same number of oxygen vacancies (~14%) on the O2 site as the air-annealed undoped compound.

The RS subsystem therefore appears to be responsible for all the flexibility of this compound, with the H subsystem (which shows no sign at all of oxygen vacancies or cation doping) responsible for maintaining its structural integrity.

Acknowledgments

Synchrotron XRD data were collected at the Australian National Beamline Facility (ANBF) by A/Prof Brendan Kennedy of the University of Sydney, with support from the Australian Synchrotron Research Program (ASRP), which is funded by the Commonwealth of Australia under the Major National Research Facilities Program.

References

[1] S.W. Li, R. Funahashi, I. Matsubara, K. Ueno, H. Yamada, J. Mater. Chem. 9 (1999) 1659.
[2] S.W. Li, R. Funahashi, I. Matsubara, K. Ueno, S. Sodeoka, H. Yamada, Chem. Mater. 12 (2000) 2424.
[3] A.C. Masset, C. Michel, A. Maignan, M. Hervieu, O. Toulemonde, F. Studer, B. Raveau, J. Hejtmanek, Phys. Rev. B 62 (2000) 166.
[4] J. Sugiyama, J.H. Brewer, E.J. Ansaldo, H. Itahara, K. Dohmae, Y. Seno, C. Xia, T. Tani, Phys. Rev. B 68 (2003) 134423.
[5] J. Sugiyama, C.T. Xia, T. Tani, Phys. Rev. B 67 (2003) 104410.
[6] D. Grebille, S. Lambert, F. Bouree, V. Petricek, J. Appl. Crystallogr. 37 (2004) 823.
[7] S. Lambert, H. Leligny, D. Grebille, J. Solid State Chem. 160 (2001) 322.
[8] Y. Miyazaki, M. Onoda, T. Oku, M. Kikuchi, Y. Ishii, Y. Ono, Y. Morii, T. Kajitani, J. Phys. Soc. Japan 71 (2002) 491.
[9] N.E. Brese, M. O'Keeffe, Acta Crystallogr. B 47 (1991) 192.
[10] T. Mizokawa, L.H. Tjeng, H.-J. Lin, C.T. Chen, R. Kitawaki, I. Terasaki, S. Lambert, C. Michel, Phys. Rev. B 71 (2005) 193107.
[11] M. Karppinen, H. Fjellvåg, T. Konno, Y. Morita, T. Motohashi, H. Yamauchi, Chem. Mater. 16 (2004) 2790.
[12] Y. Morita, J. Poulsen, K. Sakai, T. Motohashi, T. Fujii, I. Terasaki, H. Yamauchi, M. Karppinen, J. Solid State Chem. 177 (2004) 3149.
[13] J. Shimoyama, S. Horii, K. Otzschi, M. Sano, K. Kishio, Jpn. J. Appl. Phys. 42 (2003) L194.
[14] B.C. Zhao, Y.P. Sun, W.J. Lu, X.B. Zhu, W.H. Song, Phys. Rev. B 74 (2006) 144417.
[15] B.C. Zhao, Y.P. Sun, W.H. Song, J. Appl. Phys. 99 (2006) 073906.
[16] S. Li, X.Y. Qiu, Y.J. Gu, J. Zhang, J. Appl. Phys. 99 (2006) 053709.
[17] L.B. Wang, A. Maignan, D. Pelloquin, S. Hébert, B. Raveau, J. Appl. Phys. 92 (2002) 124.
[18] C. Xia, J. Sugiyama, H. Itahara, T. Tani, J. Cryst. Growth 276 (2005) 519.
[19] H. Minami, K. Itaka, H. Kawaji, Q.J. Wang, H. Koinuma, M. Lippmaa, Appl. Surf. Sci. 197 (2002) 442.
[20] J. Nan, J. Wu, Y. Deng, C.-W. Nan, Solid State Commun. 124 (2002) 243.
[21] S. Noguchi, T. Sekimoto, T. Ishida, J. Phys.: Condens. Matter 16 (2004) S5769.
[22] R.D. Shannon, Acta Crystallogr. A 32 (1976) 751.
[23] V. Petricek, M. Dusek, L. Palatinus, Institute of Physics, Praha, Czech Republic, 2004.